Available online at www.sciencedirect.com
SCIENCE DIRECT®
ELSEVIER
Nuclear Instruments and Methods in Physics Research A 517 (2004) 189–201
NUCLEAR INSTRUMENTS & METHODS IN PHYSICS RESEARCH Section A
www.elsevier.com/locate/nima

Origin and removal of spurious background peaks in vibrational spectra measured by filter-analyzer neutron spectrometers

T.J. Udovic[a,*], D.A. Neumann[a], J. Leão[a], C.M. Brown[a,b]

[a] *NIST Center for Neutron Research, National Institute of Standards and Technology, 100 Bureau Dr., MS 8562, Gaithersburg, MD 20899-8562, USA*

[b] *Department of Materials Science and Engineering, University of Maryland, College Park, MD 20742, USA*

Received 22 August 2003; accepted 2 October 2003

Abstract

Inelastic neutron scattering is an invaluable technique for measuring the vibrational spectra of materials. One of the standard methods for analyzing the energies of neutrons scattered by vibrational modes involves the use of polycrystalline beryllium filters. Here, we demonstrate that the spurious background features between 50 and 85 meV accompanying vibrational spectra measured with filter-analyzer neutron spectrometers are due to phonon excitations of the beryllium filter. These features are significantly reduced by an auxiliary polycrystalline bismuth filter placed in front of the main filter. Such a bismuth filter can result in only a minor attenuation in sample scattering intensity concomitant with a reduction in the thermal- and fast-neutron background from the sample.

PACS: 29.30.Hs; 29.30.−h; 25.40.Fq; 25.40.Dn

Keywords: Beryllium filter; Bismuth filter; Lead filter; Neutron scattering; Total cross section; Vibrational spectroscopy

1. Introduction

Ever since Brockhouse et al. [1–3] introduced the "beryllium detector method" over four decades ago, filter-analyzer-type neutron spectrometers have been invaluable for characterizing the vibrational density of states (VDOS) of materials. An example of such a spectrometer is the new Filter-Analyzer Neutron Spectrometer (FANS) at the NIST Center for Neutron Research (NCNR), shown schematically in Fig. 1. Typical of reactor-based instruments, a collimated beam of monoenergetic neutrons is extracted from a white beam using a crystalline monochromator and directed onto the sample. The scattered neutrons that reach the detectors must first pass through a low-energy bandpass filter, which ideally removes all neutrons with final energies above a Bragg cutoff energy that is intrinsic to the filter material. This cutoff occurs because neutrons with

*Corresponding author. Tel.: +1-301-975-6241; fax: +1-301-921-9847.

E-mail address: udovic@nist.gov (T.J. Udovic).

0168-9002/$ - see front matter © 2003 Elsevier B.V. All rights reserved.
doi:10.1016/j.nima.2003.10.083

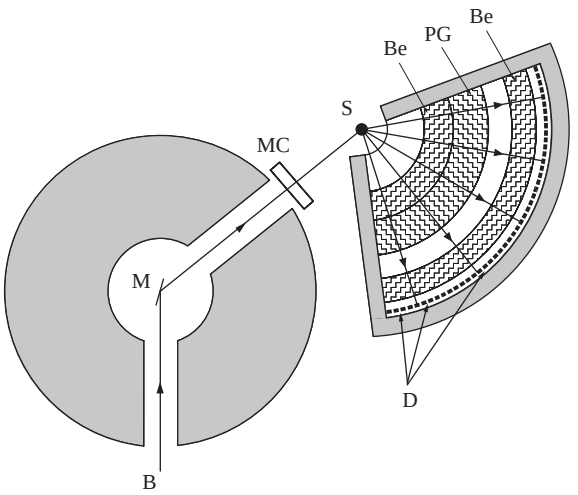

Fig. 1. A schematic diagram of the Filter-Analyzer Neutron Spectrometer (FANS) at the NIST Center for Neutron Research indicating the incident neutron beam (B), monochromator (M), monitor counter (MC), sample (S), Be and pyrolytic graphite (PG) filters, and detectors (D). The setup is basically the same as that of the instrument described in Ref. [3].

wavelengths longer than twice the maximum interplanar d spacing cannot satisfy the Bragg condition and are therefore transmitted with no attenuation due to Bragg scattering. On the other hand, shorter-wavelength neutrons are strongly attenuated [4]. Thus, the average energy, E_f, of the neutrons that traverse the filter unscattered is largely determined by the Bragg cutoff. By scanning the incident energy, E_i, one obtains a spectrum of neutron intensity as a function of neutron energy loss $E = E_i - E_f$. This spectrum directly reflects the VDOS of the sample under study, weighted by the neutron cross section for the elements in the material [3,5].

Often, the filter material used in these spectrometers is polycrystalline beryllium, the original choice of Brockhouse et al. [1–3]. Beryllium possesses many attributes that make it a seemingly ideal choice, including a small absorption cross section, a small incoherent-scattering cross section, and a rather hard phonon spectrum that tends to reduce the thermal diffuse scattering. When combined, these attributes lead to a very high transmission for the desired low-energy neutrons. However, beryllium has a Bragg cutoff energy of ≈ 5 meV. In typical implementations, this translates to an average final energy $E_f \approx 3$ meV and a somewhat large, Gaussian-equivalent, energy-resolution contribution of ≈ 4 meV full-width at half-maximum (FWHM). This resolution can be improved substantially to ≈ 1.1 meV FWHM by using polycrystalline graphite (which has a Bragg cutoff energy of ≈ 1.8 meV) as the filter material, albeit at the expense of reduced intensity. As implemented on FANS, the use of polycrystalline graphite results in an average final energy $E_f \approx 1.2$ meV. Because beryllium acts as a better filter than graphite alone for removing the majority of neutrons with energies above 5 meV, the graphite in FANS is actually sandwiched between two polycrystalline beryllium layers (see Fig. 1). The sandwich geometry was chosen since it was empirically shown to reduce more effectively the fast-neutron background, thus leading to an improved signal-to-noise ratio [6]. The entire filter assembly is routinely maintained at a temperature below ≈ 90 K with liquid nitrogen to minimize intensity losses from phonon scattering in the filter materials.

For many neutron vibrational spectroscopy (NVS) measurements, the background is relatively featureless compared to the main vibrational modes. Yet, upon closer scrutiny, particularly for samples with a VDOS entirely below 50 meV, it is evident that spurious scattering exists between 50 and 85 meV. In fact, these features can be of similar or even greater magnitude than the VDOS from weakly scattering samples, significantly contaminating the desired spectrum.

Here, we demonstrate that these ubiquitous features of all filter-analyzer-type neutron spectrometers are due to Be-phonon excitations in the filter analyzer caused by neutrons elastically scattered from the sample. Moreover, we show that this scattering can be easily reduced by one to two orders of magnitude by the addition of a polycrystalline-bismuth filter layer placed in front of the main filter. This greatly improves the capabilities of the filter-analyzer technique for probing dilute or weakly scattering systems with VDOS in the 50–85 meV region.

2. Experimental details

All samples and filter materials had a metals purity $\geqslant 99.99$ at%. The majority of the VDOS measurements were taken on FANS using two monochromators, Cu(2 2 0) for energy transfers between 25 and 250 meV and pyrolytic graphite PG(0 0 2) for energy transfers between 4 and 45 meV. Horizontal collimations before and after the monochromators were varied from 20′ to 60′ of arc depending on the desired instrumental resolution. The FWHM resolutions associated with all displayed spectra are depicted by horizontal bars beneath the spectra. Two low-energy VDOS measurements were taken on the Fermi-Chopper Time-of-Flight Spectrometer (FCS) [7] using neutron energy gain with 6 Å (2.27 meV) incident neutrons. Lead and bismuth transmission measurements were taken on the Disk-Chopper Time-of-Flight Spectrometer (DCS) [7,8] using a pulsed white beam of cold neutrons with 56 μs FWHM pulse widths, a 10 mm diameter beam cross section (as defined by a Cd mask), and 30 ms between pulses. The distances from pulse origin and sample position to neutron monitor were ≈ 2.0 and 0.5 m, respectively. The active cross section of the neutron monitor was 30 mm wide by 100 mm high. A room-temperature bismuth diffraction pattern was measured on the BT-1 high-resolution neutron powder diffractometer [9] using 1.5401 Å neutrons from the Cu(3 1 1) monochromator with horizontal divergences of 15′, 20′, and 7′ of arc for the in-pile, monochromatic-beam, and diffracted-beam collimators, respectively.

3. Results and discussion

Figs. 2(a)–(d) display representative FANS spectra for a variety of materials: coarsely polycrystalline Bi, polycrystalline V, polycrystalline $NbN_{0.007}H_{0.004}$ [10], and nanocrystalline Pd [11]. The latter two samples were measured with the old FANS instrumental configuration [4] in the low-resolution mode using only a Be filter (i.e., no graphite filter) in conjunction with a much smaller detector solid angle. For all these materials, the acoustic VDOS is known to be located well below

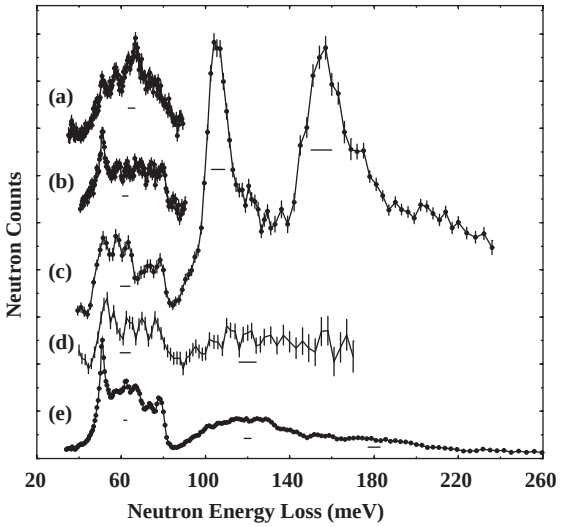

Fig. 2. FANS spectra of (a) coarsely polycrystalline Bi (295 K), (b) polycrystalline V (295 K), (c) polycrystalline $NbN_{0.007}H_{0.004}$ (4.2 K) from Ref. [10], (d) nanocrystalline Pd (10 K) from Ref. [11], and (e) polycrystalline Be (295 K). Each spectrum is normalized and vertically offset appropriately to aid visually in their comparison.

50 meV. For $NbN_{0.007}H_{0.004}$, the additional hydrogen optic VDOS is known to be located above 85 meV as evidenced by the two intense bands at ≈ 105 and 157 meV [10]. Despite this, all the measured spectra exhibit unexpected spurious multipeak scattering between 50 and 85 meV. A comparison of the different spectra in this region indicates similarities in the positions of the peaks, yet with variations in their relative intensities. The fact that the energy envelope of this scattering is independent of the sample suggests that it originates in the filter analyzer itself. Since it has been determined that both Be and Be–graphite–Be composite filters yield the same unwanted features, beryllium was the suspected source. Hence, two questions must be answered. First, by what mechanism is the beryllium creating these spurious peaks? Second, what type of scattered neutrons are involved?

The previously reported phonon-dispersion curves for beryllium [12] provided the definitive clue, notably that the range of Be-phonon energies spans from 51 to 84 meV, virtually identical to the energy range of the observed spurious scattering.

This suggested that the spurious scattering arises from *Be-phonon excitations in the filter analyzer*. Moreover, assuming that the final energies of the spurious neutrons are determined by the low-energy bandpass filter implies that the energy of the neutrons that strike the filter (i.e., before Be-phonon excitation) must be identical to the energy of the neutrons incident on the sample. Hence, the neutrons responsible for the spurious features must be *elastically scattered from the sample*. Thus, the sample is the origin of a secondary beam that impinges on the analyzer. While the vast majority of these neutrons are also elastically scattered by the filter materials and removed by neutron absorbing material, a small fraction are inelastically scattered by phonons in the polycrystalline Be layer closest to the sample and are then able to pass through the rest of the filter analyzer to the detectors.

To verify this explanation, a large block of polycrystalline beryllium ($63 \times 63 \times 51$ mm) was centered at the sample position with one long dimension parallel to the 25×63 mm ($w \times h$) incident beam and the other long dimension vertically aligned. This was meant to mimic, to first order, the relatively thick Be-filter material that the scattered elastic neutrons from a typical sample would encounter. The resulting room-temperature FANS spectrum is shown in Fig. 2(e). The similarity between the beryllium VDOS and the spurious scattering in Fig. 2 confirms that these unwanted features arise from inelastic scattering in the Be filter. Moreover, it is clear from the very broad, relatively featureless, higher-energy bands originating from multiple inelastic scattering within the thick beryllium block and evident near $\approx$120 and 180 meV in Fig. 2(e), that similar higher-energy spurious scattering is also present in all FANS spectra. This is corroborated by the broad spurious band at $\approx$120 meV for nanocrystalline Pd in Fig. 2(d).

The sample-dependent differences in the intensities of the various spurious features occurs because the elastic scattering from the sample depends on the incident energy as well as the magnitude of its coherent and incoherent neutron scattering cross sections. In particular, for coherent elastic scattering, the intensity depends on the incident neutron energy because the amount of Bragg scattering varies with the incident neutron wavelength. For the polycrystalline V sample in Fig. 2(b), the coherent scattering cross section is negligible. Thus, there are no coherent scattering effects on the shape, and the resulting spurious spectrum looks very similar to the polycrystalline-beryllium VDOS in Fig. 2(e), especially since both were measured under the same high-resolution conditions with the new FANS instrument. For polycrystalline $NbN_{0.007}H_{0.004}$ (Fig. 2(c)) and nanocrystalline Pd (Fig. 2(d)), the Debye–Scherrer rings of Bragg scattering from the sample cause subtle differences in the shape of the resulting spurious scattering, causing sample-dependent deviations from Fig. 2(e). The $NbN_{0.007}H_{0.004}$ sample has the added complication that there is probably some minor scattering contribution in the 50–85 meV region from the nitrogen optical VDOS. Finally, since the Bi sample is almost totally a coherent scatterer and was comprised of only a few single crystals, the coherent scattering effects will be more dramatic with only directed beams of Bragg-scattered neutrons contributing to the Be-filter phonon excitations. The result is seen in Fig. 2(a), where the shape of the spurious scattering deviates markedly from the other samples.

In practice, beryllium is not the first material that the elastically scattered neutrons encounter on their way toward the FANS detectors. The Be filter is cooled in a vacuum-evacuated chamber with an aluminum window between the Be and the sample. Moreover, there are usually more Al windows that exist between any given sample and the first Be filter, depending on the sample container and the particular temperature-regulating device that is used to house it. Hence, besides the relatively strong Be-filter phonon excitations between 50 and 85 meV, it is interesting to observe that the additional small scattering feature evident at 36 meV for Bi in Fig. 2(a) most likely represents the excitation of spurious aluminum phonons from the filter window. Depending on the particular experimental conditions, one may have to consider the importance of this extra spurious Al scattering when analyzing a particular FANS spectrum.

Since the front beryllium layer is not a perfect filter for stopping the elastically scattered neutrons from the sample, there is no way to avoid some spectral contamination between 50 and 85 meV, whose intensity will be proportional to the number of elastically scattered neutrons, regardless of the sample composition. Therefore, the only way to attenuate this undesirable background scattering is to attenuate the number of elastically scattered neutrons that impinge on the Be filter. One way to do this is to add another attenuating filter layer in front that is composed of a material (most likely one of the heavier elements) with a VDOS located much lower than the energies of interest, far removed from the crucial 50–85 meV region. Then, instead of spurions from Be-phonon excitations, one would get new spurions from the lower-energy phonons of the new material.

Of all the heavy-element materials, only polycrystalline ^{208}Pb (which has an abundance of 52.4% in natural lead) and ^{209}Bi (which is the only isotope in natural bismuth) appear to possess the required filter properties, i.e., sufficiently low neutron absorption cross section and sufficiently high coherent neutron scattering cross section, relatively low phonon energies, and higher Bragg cutoff energies than that of the pyrolytic graphite filter. Table 1 compares the key properties of the various lead and bismuth isotopes. Although it seems like ^{208}Pb would be a better filter choice from the viewpoint of physical properties (i.e., an almost two-orders-of-magnitude lower neutron absorption cross section, $\approx$24% higher coherent neutron scattering cross section, $\approx$16% higher molar density, and a 4 meV lower phonon cutoff energy of 9.1 meV), the existence of other much more highly neutron-absorbing lead isotopes in natural lead, namely ^{207}Pb (22.1% abundance) and ^{204}Pb (1.4% abundance), discourages the use of natural lead. The only way that a polycrystalline lead filter would be favorable would be to use pure ^{208}Pb or ^{207}Pb-depleted natural lead. Both of these options are currently cost-prohibitive. Thus, from a practical viewpoint, polycrystalline bismuth (i.e., 100% ^{209}Bi) was determined to be the only favorable candidate. It has a high attenuation for neutrons with energies >1.9 meV (compared to the 1.8 meV Bragg cutoff energy for graphite), a low attenuation for neutrons with energies <1.9 meV, and a favorable phonon cutoff energy of 13.2 meV.

Fig. 3 illustrates the VDOS spectra for coarsely polycrystalline Pb and Bi at 295 K as measured by both FANS and FCS, confirming the low phonon

Table 1
Key filter properties of the naturally occurring lead and bismuth isotopes

Isotope	% Natural abundance	Neutron cross-sections (b)[a]				Molar density (kmol/m^3)[b]	Phonon cutoff energy (meV)[b]	Bragg cutoff energy (meV)[b]
		Coherent scattering	Incoherent scattering	Total scattering	Absorption			
Pb	100	11.115	0.003	11.118	0.171	54.76	9.1	2.50
^{204}Pb	1.4	12.3	0	12.3	0.65			
^{206}Pb	24.1	10.68	0	10.68	0.03			
^{207}Pb	22.1	10.82	0.002	10.82	0.699			
^{208}Pb	52.4	11.34	0	11.34	0.00048	$\approx$54.97	$\approx$9.1	$\approx$2.50
^{209}Bi	100	9.148	0.0084	9.156	0.0338	46.93	13.2	1.90[c]

Isotopic abundances and neutron scattering and absorption cross-sections are taken from Ref. [19]. Molar densities are taken from Ref. [20]. Phonon cutoff energies are taken from Refs. [21–23]. Bragg cutoff energies are calculated from room temperature structural parameters from Refs. [15,16].

[a] All scattering cross-sections are bound cross-sections. Absorption cross-sections are for 25 meV neutrons (note: $1\,\text{b} = 1 \times 10^{-28}\,\text{m}^2$).

[b] The molar density and phonon and Bragg cutoff energies for Pb^{208} are estimated from the values reported for natural lead.

[c] Pseudo-Bragg cutoff energy. The Bi unit-cell symmetry (R-3m) [16] actually yields two minor reflections (see Fig. 5) corresponding to lower Bragg cutoff energies of 1.31 and 1.46 meV, evidenced by a small step in the total cross-section curve for polycrystalline Bi in Fig. 4.

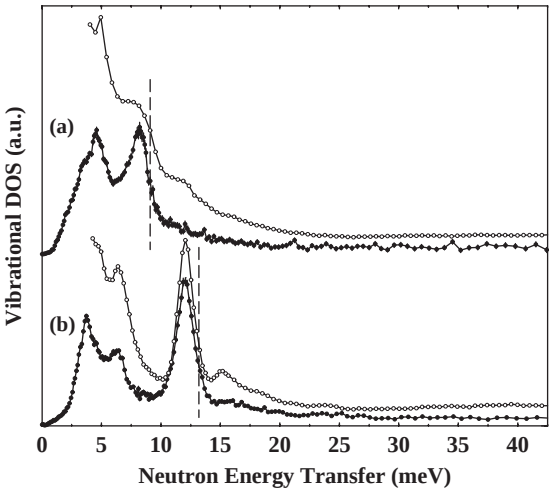

Fig. 3. VDOS spectra for coarsely polycrystalline (a) Pb and (b) Bi at 295 K measured with FANS (○) and the Fermi-Chopper Time-of-Flight Spectrometer (●). The vertical dashed lines represent the respective Pb and Bi phonon cutoff energies. Each spectrum is normalized and vertically offset appropriately to aid visually in their comparison.

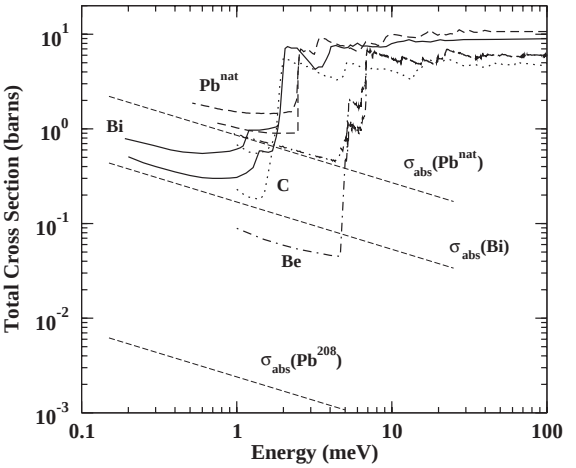

Fig. 4. The neutron energy dependence of the total cross sections of key polycrystalline filter materials, each at two temperatures (i.e., near room temperature and at cryogenic temperature): Be (296 K, 100 K) [13,14], C (graphite at 296 K, 100 K) [4,13], Bi (300 K, 100 K) [13,14], and Pb (296 K, 109 K) (this study and Ref. [13]). For each pair of curves, the one with the higher cross section (below the Bragg cutoff energy) corresponds to the higher temperature. Dashed lines represent the absorption cross section contributions to the total cross section for Bi, natural Pb, and pure ^{208}Pb. Note: $1\,b = 1 \times 10^{-28}\,m^2$.

cutoff energies reported in Table 1. The Pb and Bi samples were ≈7 and 10 mm thick, respectively, and the resulting spectra show clear evidence of additional, minor, multiple-inelastic-scattering intensity above the phonon cutoff energies, similar to the behavior seen for the thick Be sample in Fig. 2(e) above. Although minor, such multiple-scattering features will most likely contribute to the overall spurious scattering intensity resulting from any auxiliary Bi or ^{208}Pb filter and should be taken carefully into consideration when analyzing VDOS spectra of weakly scattering samples in this region.

Fig. 4 compares the energy dependence of the total cross sections for polycrystalline beryllium, graphite, bismuth, and lead (adapted in part from Refs. [4,13,14]), indicating the respective Bragg cutoff energies mentioned earlier. The marked decrease in total cross sections with decreasing temperature for neutron energies below the Bragg cutoff energies is the reason why it is desirable to operate the FANS filter near liquid nitrogen temperature.

The total cross section for polycrystalline natural lead at 295 K in Fig. 4 was determined from measurements on DCS using a 10 mm thick compressed powder sample with an average crystallite size less than 150 μm. The 109 K cross section curve at low energies was adapted from Ref. [13]. The Bragg cutoff energy for Pb at ≈2.5 meV corresponds to the (1 1 1) reflection (with a d spacing of 2.858 Å) of the Fm3m-symmetric lattice with a 298 K lattice constant $a = 4.9508$ Å [15]. Besides being the lowest-angle reflection, it also possesses the most neutron diffraction intensity. Although Fig. 4 indicates that natural lead near 100 K would be a "possible" candidate as a front auxiliary filter, the approximately three-fold higher total cross section below 1.9 meV (due to high ^{207}Pb and ^{204}Pb absorption cross sections) compared to bismuth renders it a poor second choice unless isotopically pure ^{208}Pb or ^{207}Pb-depleted natural lead is used. Since the absorption cross section is the major contributor to the total cross section below the Bragg cutoff energy, the roughly 70-fold lower absorption cross section for pure ^{208}Pb compared to natural lead plotted in Fig. 4 illustrates the highly favorable effect that using pure ^{208}Pb would have for

reducing the total neutron cross section in this region.

Fig. 5 illustrates the three lowest neutron diffraction reflections, with the hexagonal indices (0 0 3), (1 0 1), and (0 1 2), measured for coarsely polycrystalline Bi ($\approx$15 mm thickness) at 295 K with the BT-1 powder diffractometer. Bismuth possesses R-3m symmetry with lattice constants $a = b = 4.546$ Å and $c = 11.862$ Å at 298 K [16]. The largest neutron powder diffraction peak (by over a factor of 2) is the (1 0 2) reflection, which corresponds to a d spacing of 3.280 Å and the main Bragg cutoff energy of 1.90 meV in Fig. 4. Yet this is actually not the lowest-angle reflection for Bi as evidenced in Fig. 5. The relatively small (0 0 3) peak ($d = 3.954$ Å) and even smaller (1 0 1) peak ($d = 3.737$ Å) correspond to additional Bragg cutoff energies of 1.31 and 1.46 meV, respectively. The relative neutron powder diffraction intensities expected for the (0 0 3), (1 0 1) and (0 1 2) reflections for nontextured, finely polycrystalline Bi are 4.5:1.4:100, respectively, indicating the minor importance of the two lowest-angle reflections. These are not exactly the intensity ratios observed for the Bi powder pattern in Fig. 5. Yet, this is to be expected since the sample consisted of a small number of fairly large crystallites resulting in a highly textured material. In fact, the asymmetric shape of the (0 1 2) reflection is clear evidence that the sample is not representative of a finely polycrystalline material. Although of minor importance, the presence of the (0 0 3) reflection is indeed manifested by the small step observed in the total neutron cross section for polycrystalline Bi near 1.3 meV in Fig. 4. Since this step occurs below the 1.8-meV graphite cutoff energy, it may lead to a slight improvement in the limiting resolution of any composite filter analyzer that includes Bi.

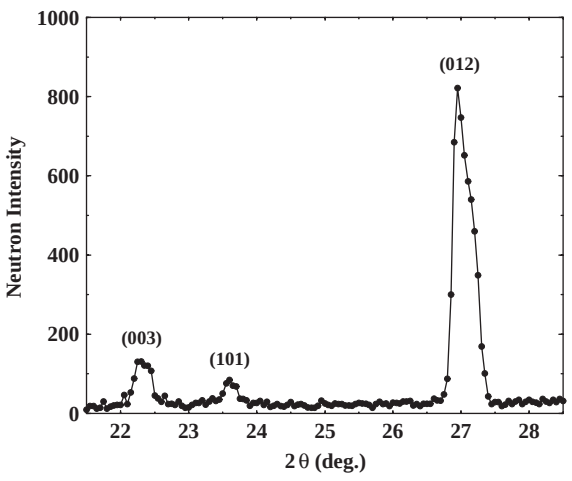

Fig. 5. The three lowest neutron diffraction peaks (labeled with hexagonal indices) for coarsely polycrystalline Bi at 295 K measured on the BT-1 powder diffractometer.

The results of transmission calculations based on the energy-dependent total cross sections for polycrystalline bismuth are illustrated in Fig. 6. Estimated transmissions for representative Bi-filter thicknesses are summarized in Table 2. The transmission, T, for the Bi filter is defined as

$$T = I/I_o = \exp(-\sigma n t) \quad (1)$$

where I_o and I are the incident and transmitted neutron intensities, respectively, σ is the total neutron cross section per atom, n is the atom density, and t is the filter thickness. These results indicate that even a 100-mm-thick bismuth layer at room temperature is enough to attenuate the elastically scattered neutrons by more than an

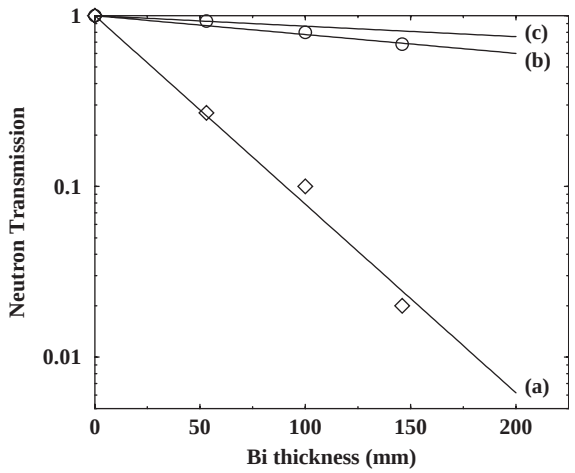

Fig. 6. Calculated polycrystalline-bismuth transmissions vs. thickness, assuming total neutron cross sections estimated from Fig. 4 for (a) elastically scattered neutrons above 50 meV [$\sigma \approx 9$ b], and neutrons below the Bragg cutoff energy with the Bi filter at (b) 300 K [$\sigma \approx 0.9$ b] and (c) 100 K [$\sigma \approx 0.5$ b]. Data points correspond to transmissions determined experimentally from the FANS measurements in Figs. 9–11 and summarized in Table 2.

Table 2
Estimated attenuation of Be-filter spurion and signal intensities for various polycrystalline-Bi-filter thicknesses based on the total neutron cross-sections for polycrystalline Bi [13,14] displayed in Fig. 4

Bi-filter thickness (mm)	Be spurions (I/I_o) (calc.)[a]	Signal (100 K) (I/I_o) (calc.)[b]	Signal (300 K) (I/I_o) (calc.)[c]	Be spurions (I/I_o) (exp.)[d]	Signal (295 K) (I/I_o) (exp.)[e]
0	1	1	1	1	1
53	0.26	0.93	0.87	0.27	0.93
100	0.079	0.87	0.78	0.1	0.80
146	0.024	0.81	0.69	0.02	0.68
200	0.0062	0.75	0.60		

[a] Assuming $\sigma = 9$ b.
[b] Assuming $\sigma = 0.5$ b.
[c] Assuming $\sigma = 0.9$ b.
[d] Based on scale factors used in Fig. 9.
[e] Based on fits of spectra in Figs. 10 and 11.

order of magnitude while $\approx$80% of the neutrons whose wavelengths are below the Bragg cutoff are transmitted through the filter. Moreover, cooling the bismuth below 100 K would increase the transmission of the desirable low-energy neutrons to near 90%. Hence, an additional 100-mm-thick, liquid-nitrogen-cooled, polycrystalline-bismuth layer could remove more than 90% of the spurious intensity in the 50–85 meV region while retaining $\approx$90% of the vibrational signal. Since the total neutron cross section for bismuth remains high for fast neutrons, it is likely that the fast-neutron background would be reduced as well by adding a bismuth filter.

Fig. 7 compares the neutron energy dependence of the total cross section at room temperature for polycrystalline Bi (from Ref. [13]) and single-crystal Bi. The latter was measured on DCS using a 5 cm thick, single-crystal sample and is consistent with previously reported results [17]. Although there is no sharp Bragg cutoff energy, it is clear that even single-crystal bismuth should be an acceptable FANS filter to remove spurious Be-filter phonon features. The only critical energy regions in Fig. 7 are above 50 meV, where the beryllium phonon energies are located, and below 1.8 meV, which is the Bragg cutoff energy for graphite. Therefore, since the total cross sections for neutrons above 50 meV are sufficiently large, such materials would still be effective for attenuating the elastically scattered neutrons that would undergo spurious beryllium phonon scattering.

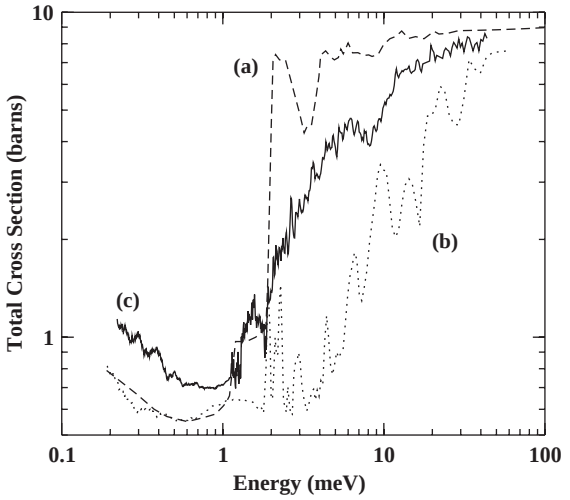

Fig. 7. The neutron energy dependence of the room-temperature total cross section for (a) polycrystalline Bi (from Ref. [13]) compared with that of (b) single-crystal Bi and (c) the prototype, coarsely polycrystalline Bi filter, both determined from transmission measurements on DCS as described in the text.

Since the ultimate resolution is derived from the filtering action (i.e., the Bragg cutoff energy) of the polycrystalline-graphite layer, it is not necessary for the Bi filter to possess such a sharp Bragg cutoff edge. Rather, it is sufficient that the total cross section be relatively low below 1.8 meV (as is the case) to minimize the attenuation of the inelastically scattered neutrons from the sample.

With these expectations in mind, a prototype, room-temperature, coarsely polycrystalline, bismuth filter was constructed for testing purposes, permitting a variable filter thickness between 0 and 146 mm. The bismuth-filter material was machined from poured Bi ingots. These ingots typically possessed relatively large single-crystal domains with average dimensions of the order of 5–10 mm. The final filter had a 70×70 mm cross section and was composed of several individual sections. The filter thickness was varied by the appropriate addition or subtraction of these sections. The filter was positioned inside a 70×70 mm square-cross section Cd tube (with 0.6-mm wall thickness) that was 150 mm in length. The Cd tube provided an orifice of constant solid angle for detection of neutrons scattered by the sample, independent of the filter thickness. Moreover, it acted as an absorber of thermal neutrons scattered by the filter. The neutron energy dependence of the total cross section of this prototype Bi filter was determined from transmission measurements performed on DCS for a filter thickness of 146 mm. The resulting total cross section curve is plotted in Fig. 7 for comparison with those for polycrystalline and single-crystal Bi. This comparison corroborates the coarsely crystalline morphology of the prototype Bi filter. The total cross section values above 50 meV and below 1.9 meV correspond favorably to the estimated transmission lines in Fig. 6.

Although a filter material with much finer than centimeter-sized crystallite domains was ultimately more preferable, the synthesis of such a fine-grained material was nontrivial, requiring more advanced powder-metallurgy techniques. Hence, the current prototype filter was a first attempt with commercially available bismuth to test the viability of the concepts proposed. Following from the total cross section data in Fig. 7 and the discussion above, it is evident that such a filter provided a useful lower limit for the efficiency for removing the "undesirable" elastically scattered neutrons as well as for transmitting the "desirable" inelastically scattered neutrons. The setup is depicted schematically in Fig. 8.

Figs. 9–11 display FANS spectra of coarsely polycrystalline Bi, polycrystalline V, and single-crystal $NbD_{0.6}$, respectively, before and after the addition of various bismuth filter thicknesses to the front of the filter analyzer. For each material, it

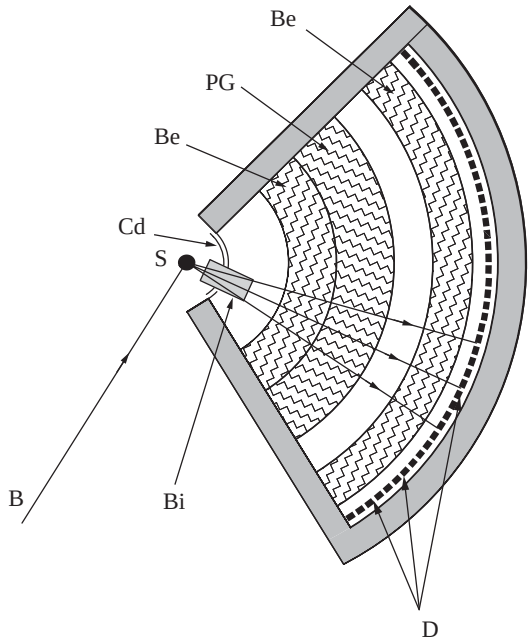

Fig. 8. A schematic diagram of the FANS filter-analyzer test setup with the additional, prototype, coarsely polycrystalline, bismuth-filter layer, as described in the text.

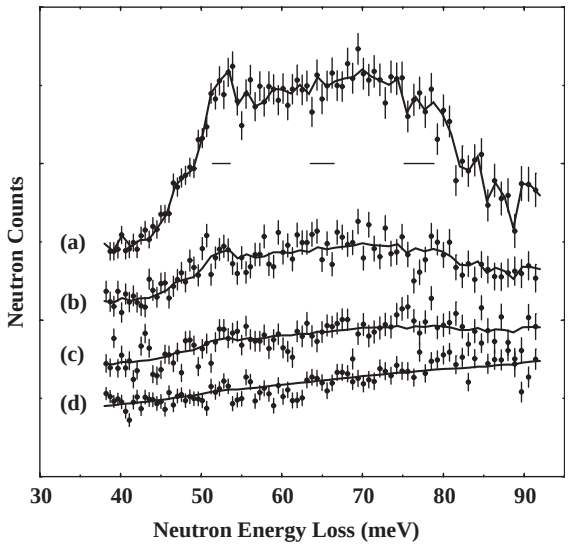

Fig. 9. Room-temperature FANS spectrum of Bi with (a) 0 mm, (b) 53 mm, (c) 100 mm, and (d) 146 mm thick, prototype, bismuth filter added to the front of the filter analyzer.

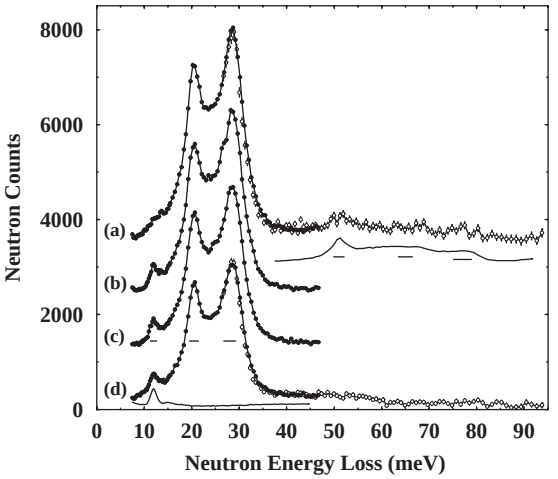

Fig. 10. Room-temperature FANS spectrum of V with (a) 0 mm, (b) 53 mm, (c) 100 mm, and (d) 146 mm thick, prototype, bismuth filter added to the front of the filter analyzer. Overlapping data points were measured with the PG(0 0 2) (●) and Cu(2 2 0) (○) monochromators. All spectra are normalized to the same neutron monitor counts. For clarity, each successive V spectrum above the bottom spectrum is offset vertically from the previous spectrum by 1000 additional neutron counts. Solid lines plotted below the V data represent the corresponding room-temperature FANS spectra for bismuth (lower-energy curve) and beryllium (higher-energy curve) for comparison.

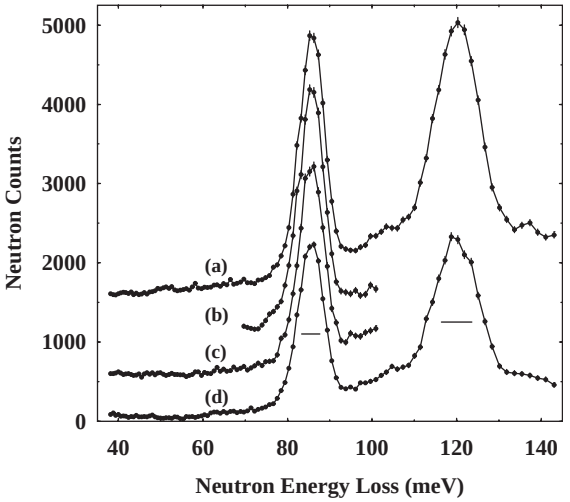

Fig. 11. Room-temperature FANS spectrum of $NbD_{0.6}$ with (a) 0 mm, (b) 53 mm, (c) 100 mm, and (d) 146 mm thick, prototype, bismuth filter added to the front of the filter analyzer. Peaks at 85.5 and 120 meV are due to D optical phonons. All spectra are normalized to the same neutron monitor counts. For clarity, each successive spectrum above the bottom spectrum is offset vertically from the previous spectrum by 500 additional neutron counts.

is clear that the bismuth filter dramatically attenuates the features due to Be-filter phonons. A quantitative estimate of the attenuations of the Be-filter phonon scattering vs. Bi-filter thickness was determined from the Bi sample spectra in Fig. 9. Similarly, the corresponding attenuations of the "desirable" sample phonon scattering were determined from the VDOS spectra of V in Fig. 10 and $NbD_{0.6}$ in Fig. 11. The attenuations are completely in line with the calculated values discussed in the previous section (see Fig. 6). Comparisons are summarized in Table 2. It is clear from the V spectra in Fig. 10 that the spurious Be-filter phonons between 50 and 85 meV have been essentially removed by the 146-mm Bi filter, but they have been replaced by new spurious Bi-filter phonons at 12 meV.

Fig. 9 also illustrates an added benefit of using an auxiliary Bi filter. A closer inspection of the baseline scattering levels vs. Bi-filter thickness indicates that they decrease significantly with increasing filter thickness. For example, even after normalizing the spectrum measured with the 146-mm Bi filter to compensate for the attenuation of "desirable" sample scattering as measured in Figs. 10 and 11, the amount of baseline scattering intensity is still lower by $\approx 50\%$. This means that the Bi filter does a better job at removing monotonic thermal neutron background noise that can contribute to the overall scattering background. For weakly scattering samples, this decrease in the noise from thermal neutrons translates into significant gains in the signal-to-noise ratio.

As suggested earlier, in addition to reductions in the thermal-neutron background, an auxiliary Bi filter was also found to reduce significantly the fast-neutron background. The amount of fast-neutron background varies from experiment to experiment. Yet, typically at least half of the fast-neutron background comes from the sample scattering of fast neutrons originating from the direction of the monochromator. The Bi filter does a better job at reducing the background contribution from these neutrons. This is illustrated in

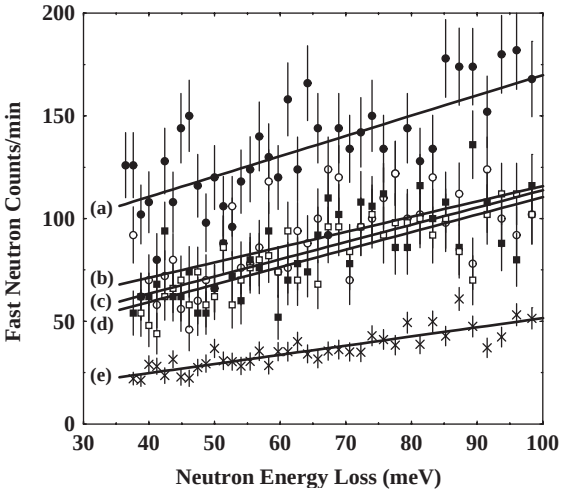

Fig. 12. Fast-neutron background intensity (counts/min) for the coarsely polycrystalline Bi sample with (a) 0 mm (●), (b) 53 mm (○), (c) 100 mm (■), and (d) 146 mm (□) thick, prototype, bismuth filter added to the front of the filter analyzer; (e) for no sample in the beam and no Bi filter (×). (Note: Using a 146 mm Bi filter yields the same result.) Measurements were taken with 60′ and 40′ horizontal collimators, respectively, before and after the Cu(2 2 0) monochromator and a 0.6-mm thick layer of cadmium placed in front of the Bi filter. Solid lines are linear fits to the data.

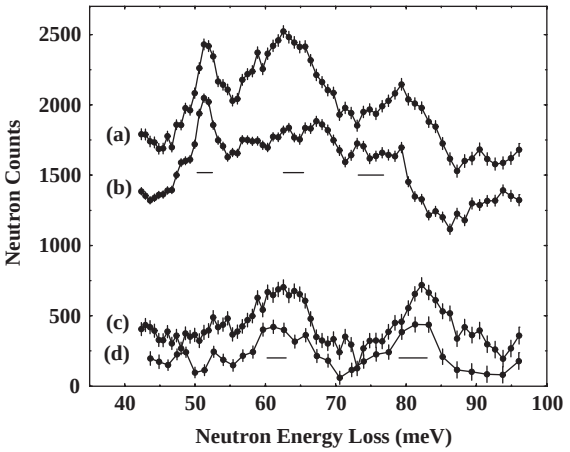

Fig. 13. FANS spectra at 10 K of a Zr–Fe–Mn–Al nitrogen getter alloy [18]: (a) with and (b) without absorbed nitrogen; (c) FANS difference spectrum {(a)–(b)} indicating two scattering features due to nitrogen optical phonons; (d) FANS spectrum of same sample as in (a) but measured at 295 K with the 146 mm thick, prototype Bi filter. Spectrum was rescaled appropriately for comparison with (c) and offset vertically by −200 counts for clarity.

Fig. 12, where the fast-neutron background intensity (counts/min) is plotted for the different Bi-filter thicknesses for the coarsely polycrystalline Bi sample. In this particular case, the data with and without the Bi sample (Figs. 12(a) and (e)) indicate that sample scattering is responsible for a dramatic 70–80% of the fast-neutron background. All Bi filter thicknesses are enough to remove ≈50% or more of the fast-neutron background contribution from the sample. There is a weak decrease of fast-neutron background with increasing Bi filter thickness between 53 and 146 mm, illustrating that even the thin, 53 mm Bi filter is sufficient to halve the fast-neutron background contribution from the sample. For the thicker 146 mm Bi filter, the attenuation of these neutrons even surpasses 60% at the lower energy transfers measured.

Again, cooling the bismuth filter below 90 K (similar to the main Be–graphite–Be composite filter) should increase the transmission of the vibrational signal due to less interference from any thermally excited bismuth phonons at this lower temperature. This is corroborated in Fig. 4 by the decrease in the polycrystalline-bismuth total cross section with decreasing temperature found for neutron energies below 1.9 meV.

In closing, Fig. 13 exemplifies the overall utility of the Bi filter for the measurement of weak scattering features that are otherwise contaminated by the spurious scattering from the Be filter. In this case, the vibrations of interest are optical phonons of nitrogen absorbed by a Zr–Fe–Mn–Al nitrogen-getter alloy [18]. Figs. 13(a) and (b) display the 10 K FANS spectra of the alloy with and without absorbed nitrogen, respectively. It is clear that a majority of the scattering in both spectra is due to spurious Be-filter phonons. Fig. 13(c) is the difference spectrum, which successfully eliminates the spurious scattering, leaving two optical phonon bands for nitrogen near 62 and 82 meV. Alternatively, Fig. 13(d) displays this same bimodal spectrum (albeit at 295 K) by remeasuring the same nitrogen-loaded alloy from Fig. 13(a), yet now using the 146 mm thick, prototype Bi filter. This illustrates that such weak phonon features can be typically extracted by a

FANS measurement without the need for subtracting off any spurious background signal that would otherwise originate from the Be filter.

4. Conclusion

The spurious background peaks between 50 and 85 meV that are characteristic of filter-analyzer-type neutron spectrometers were found to be associated with phonon excitations of the beryllium at the front of the filter analyzer by neutrons elastically scattered from the sample. These features are significantly reduced using an additional polycrystalline-bismuth layer placed in front of the main filter, even when the bismuth possesses relatively large crystallite domains. For example, an additional 100-mm-thick, coarsely polycrystalline, bismuth layer at room temperature reduces the spurious signal about an order of magnitude with only a 20% attenuation in the vibrational signal (and $\approx 10\%$ projected attenuation at 100 K) concomitant with a marked reduction in the thermal- and fast-neutron backgrounds. Increasing the filter thickness by 50% to 150 mm would reduce the spurious signal by almost two orders of magnitude with only a 30% room-temperature attenuation in the vibrational signal (and $\approx 20\%$ projected attenuation at 100 K). It should be noted that a similarly sized polycrystalline ^{208}Pb filter would probably do a better job attenuating the spurious signal with a less significant loss in vibrational signal, but such a single-isotope filter is prohibitively expensive.

By sufficiently decreasing the average crystallite domain size of the Bi filter, the total cross section for 50–85 meV neutrons will increase somewhat compared to the filter used in the present study and remain high down to the Bragg cutoff energy. This should further improve the filter efficiency for removing the spurious Be-filter phonon signal and further decrease the thermal-neutron background. In effect, a finer crystallite morphology should lead to a decrease in the required filter thickness. Ultimately, one would like to have a composite filter that maximizes both the signal/spurion and signal/background intensity ratios by optimizing the thicknesses and layout of the various filters. Nonetheless, it is clear that the addition of a bismuth filter (preferably cryocooled and more finely polycrystalline) will substantially enhance the performance of filter-analyzer spectrometers by improving their capabilities for characterizing the phonons in weakly scattering materials, free of spurious Be-filter phonon features.

Acknowledgements

The authors thank J.R.D. Copley, Q. Huang, and J.J. Rush for contributing their scientific insights. This work utilized facilities supported in part by the National Science Foundation under Agreement No. DMR-0086210.

References

[1] B.N. Brockhouse, M. Sakamoto, R.N. Sinclair, A.D.B. Woods, Bull. Am. Phys. Soc. 5 (1960) 373.
[2] B.N. Brockhouse, in: Inelastic Scattering of Neutrons in Solids and Liquids, IAEA, Vienna, 1961, p. 113.
[3] A.D.B. Woods, B.N. Brockhouse, M. Sakamoto, R.N. Sinclair, in: Inelastic Scattering of Neutrons in Solids and Liquids, IAEA, Vienna, 1961, p. 487.
[4] J.R.D. Copley, D.A. Neumann, W.A. Kamitakahara, Can. J. Phys. 73 (1995) 763.
[5] G.L. Squires, Introduction to the Theory of Thermal Neutron Scattering, Dover Publications, Inc., Mineola, NY, 1996.
[6] J.M. Rowe, J.J. Rush, unpublished results.
[7] J.R.D. Copley, T.J. Udovic, J. Res. NIST 98 (1993) 71.
[8] J.R.D. Copley, J.C. Cook, Chem. Phys. 292 (2003) 477.
[9] J.K. Stalick, E. Prince, A. Santoro, I.G. Schroder, J.J. Rush, in: D.A. Neumann, T.P. Russell, B.J. Wuensch (Eds.), Neutron Scattering in Materials Science II, Materials Research Society Symposium Proceedings No. 376, Materials Research Society, Pittsburgh, PA, 1995, p. 101.
[10] J.J. Rush, T.J. Udovic, N.F. Berk, D. Richter, A. Magerl, Europhys. Lett. 48 (1999) 187.
[11] U. Stuhr, H. Wipf, T.J. Udovic, J. Weißmüller, H. Gleiter, J. Phys.: Condens. Matter 7 (1995) 219.
[12] R. Stedman, Z. Amilius, R. Pauli, O. Sundin, J. Phys. F 6 (1976) 157.
[13] D.J. Hughes, R.J. Schwartz, Neutron Cross Sections, 2nd Edition, Brookhaven National Laboratory, Upton, NY, Report No. BNL-325, 1958.
[14] http://www.nndc.bnl.gov/nndc/exfor/
[15] H.P. Klug, J. Am. Chem. Soc. 68 (1946) 1493.

[16] P. Cucka, C.S. Barrett, Acta Crystallogr. 15 (1962) 865.
[17] B. Grabcev, S. Todireanu, V. Cioca, J. Appl. Crystallogr. 12 (1979) 399.
[18] M.A. Coleman, D. Chandra, T.J. Udovic, unpublished results.
[19] V.F. Sears, Neutron News 3 (3) (1992) 26.
[20] http://www.webelements.com.
[21] B.N. Brockhouse, T. Arase, G. Caglioti, K.R. Rao, A.D.B. Woods, Phys. Rev. 128 (1962) 1099.
[22] J.M. Rowell, W.L. McMillan, P.W. Anderson, Phys. Rev. Lett. 14 (1965) 633.
[23] J. Sosnowski, S. Bednarski, A. Czachor, in: Neutron Inelastic Scattering, Vol. I, IAEA, Vienna, 1968, pp. 157–164.